Kinetics of Cross-Polarization in Solid-State NMR: A Guide for Chemists

Waclaw Kolodziejski*,† and Jacek Klinowski*,‡

Department of Inorganic and Analytical Chemistry, Medical University of Warsaw, ul. Banacha 1, 02-097 Warszawa, Poland, and Department of Chemistry, University of Cambridge, Lensfield Road, Cambridge CB2 1EW, U.K.

Received August 7, 2000

Contents

1. Introduction

Cross-polarization (CP) from abundant spins I to dilute spins S is a double-resonance technique[1] which overcomes two common problems in the NMR of solids. The first stems from the fact that solid-state NMR of dilute nuclei, such as ^{13}C, ^{29}Si, and ^{15}N (isotopic abundance of 1.1%, 4.7%, and 0.03%, respectively), suffers from low sensitivity, particularly when these nuclei also have a low gyromagnetic ratio. As a result, in a conventional pulse-acquire solid-state NMR experiment, known as the Bloch decay (BD) experiment, very few dilute spins are actually observed. The second problem is the well-known fact that spin−lattice relaxation times of dilute spin 1/2 nuclei are usually long (tens of seconds for ^{13}C in powdered organics and minutes for ^{29}Si in framework silicates). This is because strong homonuclear dipolar interactions which can stimulate relaxation transitions are largely absent, and only the much weaker heteronuclear dipolar interactions remain. The long spin−lattice relaxation time means that long delays must be left between consecutive scans. When several thousand scans are required to lower the noise to a desirable level, the spectra take a very long time to acquire.

Cross-polarization exploits the fact that in many solids the dilute and abundant nuclei are in close proximity and are thus coupled via the magnetic dipolar interaction. CP is usually combined with magic-angle spinning (MAS) and high-power decoupling. Most pulse sequences used in solid-state NMR involve CP (Figure 1). In order for the polarization transfer to be possible, the magnetizations of spins I and S must fulfill the Hartmann−Hahn condition.[2] As CP is based on heteronuclear dipolar interactions, it is sensitive to internuclear distances and the mobility of molecules or functional groups involved. This means that CP can also be used to establish the connectivity between coupled nuclei and to monitor molecular dynamics in solids, a very useful feature in structural determination.

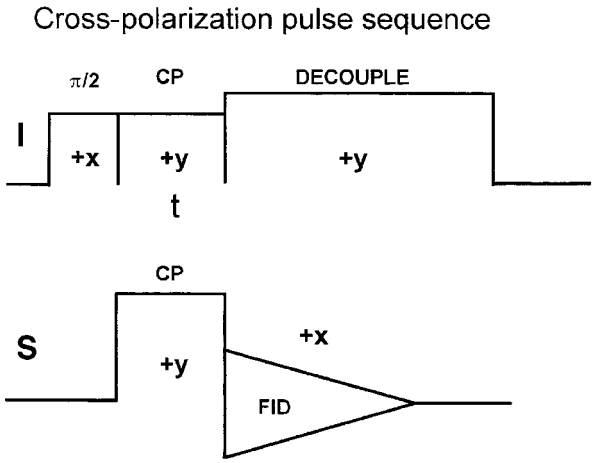

Figure 1. Basic CP pulse sequence. After the preparation period, during which the sample polarizes in the magnetic field, a $\pi/2$ pulse is applied to the I spins along the x' axis of the rotating frame. A long spin locking pulse of amplitude B_{1I} is then applied along the y' axis. At the same time, a long pulse of amplitude B_{1S} is applied to the S spins along the y' axis. This time period, during which cross-polarization takes place, is known as the contact time, t. The amplitudes of the pulses satisfy the Hartmann−Hahn condition, $\gamma_I B_{1I} = \gamma_S B_{1S}$. Finally, the radio frequency field applied to the S spins is turned off and a free induction decay of the S spins is observed.

The literature on cross-polarization solid-state NMR is growing rapidly, and a database search produced 1146 references published in the last five years alone. As many chemical studies are sometimes interpreted in terms of different theoretical treatments of CP, a comparison of the results and conclusions of different publications is often difficult. Our teaching experience indicates that there is a need for a review which would explain as simply as possible the most recent results in CP, summarize the most important theoretical approaches, point out difficulties and traps, and describe the ways in which these can be resolved or avoided.

* To whom correspondence should be addressed.
† Medical University of Warsaw. Phone: +(48)-22-57 20 784. E-mail: waclaw@pluton.farm.amwaw.edu.pl.
‡ University of Cambridge. Phone: +(44)-01223-33 65 09. Fax: +(44)-01223-33 63 62. E-mail: jk18@cam.ac.uk.

10.1021/cr000060n CCC: $39.75
Published on Web 02/05/2002

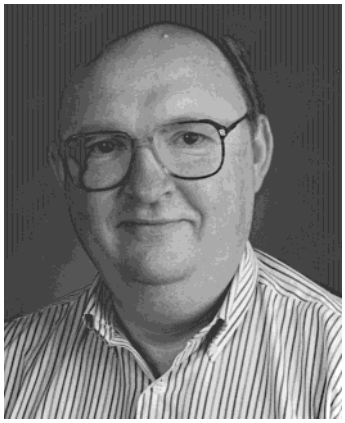

Waclaw Kolodziejski graduated in chemistry at the University of Warsaw, where he also obtained his Ph.D. degree and higher doctorate (habilitation) for work on electron spin resonance (EPR) and nuclear magnetic resonance (NMR) of molecular interactions in solutions using stable free-radical probes. He has worked on solid-state NMR since the early 1980s: at his home university, at Colorado State University, and the University of Liège (as a Postdoctoral Fellow), at Cambridge (Research Associate), and at Universidad-Politecnica de Valencia (Profesor Invitado for four years). He is now Professor of Chemistry and Head of the Department of Inorganic and Analytical Chemistry at the Warsaw Medical University. Waclaw Kolodziejski has been using NMR for the study of a very wide variety of solids and has lectured extensively on the subject. He is currently working on the characterization of bone tissue by solid-state NMR and IR microscopy. Waclaw Kolodziejski and Jacek Klinowski have collaborated for many years and have nearly 40 joint publications. (Photo reprinted with permission from Photographic Unit, University of Cambridge, Department of Chemistry, Cambridge, U.K. CB2 1EW.)

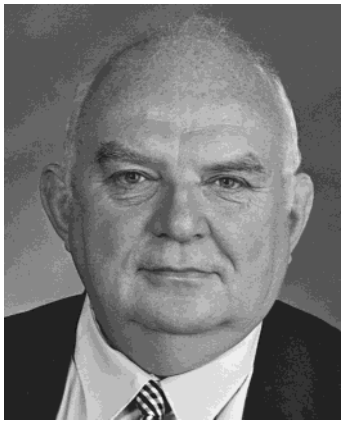

Jacek Klinowski received his Ph.D. degree from the Jagiellonian University, Kraków (where he studied chemistry and mathematics) and the University of London and and his M.A. and Sc.D. degrees from the University of Cambridge, where he is now Professor of Chemical Physics and Professorial Fellow at Peterhouse. His solid-state NMR studies involve a great variety of materials (micro- and mesoporous molecular sieves, glasses, proton sponges, minerals, ceramics, fullerenes etc.) as well as biological samples. His interests also include (i) systematic enumeration of crystalline networks using mathematical tiling theory, (ii) morphogenesis (the origin of shape and form), (iii) periodic minimal surfaces, which appear in many inorganic, organic, and biological structures, and the associated mathematical problems, and (iv) inorganic chemistry of biological systems (plant silica and alumina, the structure of bone, the interaction of silicates, such as asbestos, with tissue, Alzheimer's brain). He has over 400 publications and is the coauthor, with J. W. Hennel, of *Fundamentals of Nuclear Magnetic Resonance* (Longman, 1993) and *Primer of Magnetic Resonance Imaging* (Imperial College Press, 1998). Jacek Klinowski is Editor-in-Chief of *Solid-State Nuclear Magnetic Resonance*, an international learned journal, a Foreign Member of the Polish Academy of Arts and Sciences, a Presidential Professor, Republic of Poland, an Honorary Member of the Polish Chemical Society, a holder of the Society's Marie Curie Medal, and Visiting Professor at the Universities of Kraków and Poznan (Poland), Aveiro (Portugal), and Cagliari (Italy). (Photo reprinted with permission from Nathan Pitt, University of Cambridge, Department of Chemistry, Cambridge, U.K. CB2 1EW.)

To a chemist, CP based on the Zeeman order is of the greatest importance, and only this will be discussed here. Of course, any review inevitably presents a subjective point of view, a glance through the lens of our personal interests. Some readers may feel that too much attention has been devoted to applications in materials science or to novel CP techniques. As a number of standard texts on CP and related topics are available,[3−14] we shall not discuss the very basics of the technique but will assume some previous knowledge of the fundamental features of cross-polarization.

2. Kinetics of Cross-Polarization

2.1. Importance of the Kinetic Aspects

Users of cross-polarization will sooner or later wish to understand the kinetics and dynamics of the process and to embark upon variable-contact-time measurements. This is necessary in order to optimize the CP experiment, to obtain more complete structural information on the sample, and to make the measurements quantitative. Problems will inevitably arise as to which functions should be used to fit the kinetic data, which parameters are the most important, what is their physical meaning, and how to exploit this information in materials science and solid-state chemistry research. Knowledge of CP kinetics is crucial for the correct interpretation of CP spectra. To illustrate some of the problems involved, we give two examples from our own work.

Consider a material containing C_{70}, toluene, and C_{60} in a 100:22:9 molar ratio, with ^{13}C at natural abundance.[15,16] This is very interesting in the context of cross-polarization because it is possible to cross-polarize in both directions: $^{1}H \rightarrow {}^{13}C$ and $^{13}C \rightarrow {}^{1}H$ (Figure 2). The C_{60} carbons cross-polarize from the toluene protons and, because of the large spatial separation of the two molecular species and their substantial mobility, the optimum contact time is very long (ca. 30 ms, see Figure 3). A similar situation arises with the $^{13}C \rightarrow {}^{1}H$ experiment, which makes the cross-polarization kinetics similar in both cases. Since the probability of finding a ^{13}C nucleus in a single molecule of C_{60} is much higher than in a single molecule of toluene, the toluene protons cross-polarize from ^{13}C nuclei of C_{60}, and therefore, the $^{13}C \rightarrow {}^{1}H$ polarization transfer is very slow. By contrast, the toluene carbons cross-polarize very fast from their adjacent protons, with the optimum contact time of ca. 1 ms. Note that for $^{1}H \rightarrow {}^{13}C$ CP with 1 ms contact time, the intensity of the peaks from toluene is greatly increased compared with that of the peaks from C_{70}, and the reverse situation arises with the 30 ms contact time (Figure 3). The conclusion is that intensities of peaks within the same CP spectrum cannot be compared without a careful examination of their CP kinetics.

The second example concerns the large-pore aluminophosphate molecular sieve VPI-5 (Figure 4), which contains three crystallographically inequivalent phosphorus sites giving rise to three ^{31}P lines in the 1:1:1 intensity ratio. However, the $^{1}H \rightarrow {}^{31}P$ CP

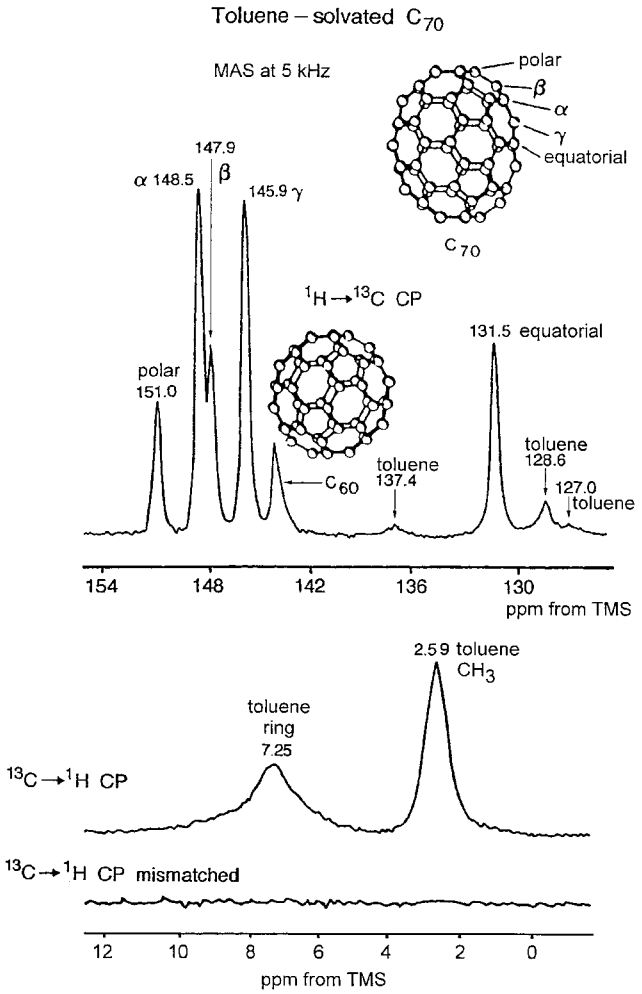

Figure 2. $^1H \rightarrow {}^{13}C$ and $^{13}C \rightarrow {}^1H$ CP spectra of toluene-solvated C_{70} (for the molecular structure see inset) recorded with a 25 ms contact time. The prominent ^{13}C lines come from the five inequivalent carbons in C_{70}. Note the ^{13}C peaks from residual C_{60} and toluene. The $^{13}C \rightarrow {}^1H$ CP spectra, shown in the absolute intensity mode, were acquired with the correct CP setup (upper spectrum) and deliberately mismatched (bottom spectrum) radio frequency fields.[15,16]

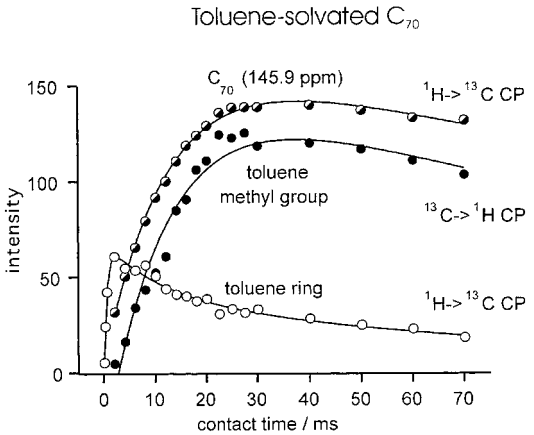

Figure 3. Comparison of CP kinetics for fullerene and toluene in toluene-solvated C_{70}.[15,16]

spectra published by various groups differed and their interpretation was a matter of much controversy. The reason for this becomes clear if one takes into account contamination from the AlPO−H3 phase,

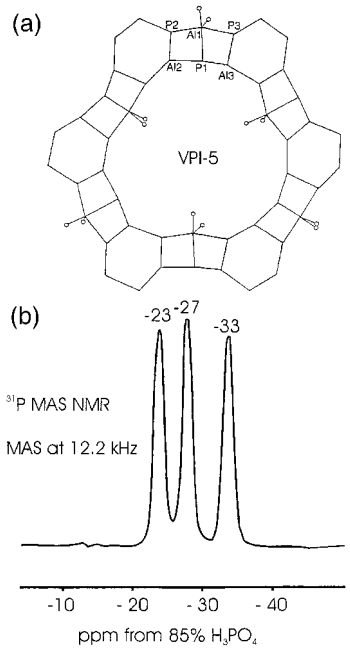

Figure 4. (a) One layer of the framework structure of hydrated VPI-5 taken from the stereoscopic view along the [001] direction showing the deviation from $P6_3cm$ symmetry. Aluminum and phosphorus atoms, linked via oxygen atoms (not shown for clarity), are located at the apexes of the polygons. Sites located between two fused four-membered rings are referred to in the text as 4−4 sites; those located between six-membered and four-membered rings are referred to as 6−4 sites. P2 and P3, and Al2 and Al3 sites are inequivalent. All Al and P atoms are linked, via oxygens, to atoms in another layer in the structure (not shown), which makes them four-coordinated, except for the Al1 site which is six-coordinated as a result of bonding to four bridging oxygens and to two "framework" water molecules. Other intracrystalline water is not shown. (b) ^{31}P Bloch-decay spectrum of VPI-5.

which cross-polarizes much more readily than does VPI-5 itself (Figure 5).[17] In the CP spectra, the peaks from AlPO−H3 at −24 and −26 ppm (in the 1:1 intensity ratio) dominate the VPI-5 peaks at −23, −27, and −33 ppm. The broad high-frequency feature comes from the P−OH groups. The conclusion is that CP can favor one compound over another, even when the former is present in low concentrations. It follows that one cannot assess the composition of a mixture without careful investigation of the CP kinetics of the entire sample and of the individual components. Quantitative conclusions can only be drawn from true peak amplitudes, calculated from the CP kinetic curves.

2.2. Classical I–S Model

Consider, for simplicity, that both spin species, I and S, have spin 1/2. Thermodynamically, such a system can be viewed as consisting of a lattice with a huge heat capacity and two subsystems, I and S, the former with a much larger heat capacity than the latter (Figure 6).[1,11] We consider the situation in terms of the inverse spin temperature β in the rotating frame.[10] We also assume that the magnetization of spins I is "locked" along the B_{1I} field, which is achieved when B_{1I} is greater than any local dipolar field. During spin lock (Figure 1) a large magnetizaton of the abundant spins I is held by a relatively

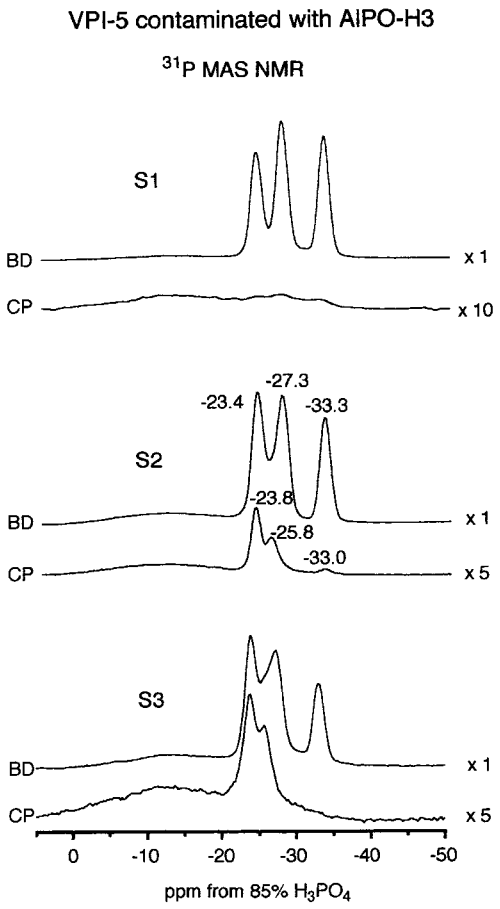

Figure 5. Comparison of ^{31}P CP and BD spectra of VPI-5 contaminated with phase AlPO−H3.[17] The content of AlPO−H3 in the samples increases in the series S1 < S2 < S3. The spectra were recorded under MAS at 7 kHz; the CP contact time was 2 ms. Note different intensity scaling factors on the right.

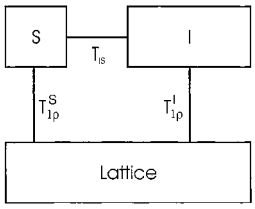

Figure 6. Block diagram of CP thermodynamics showing the lattice, the I and S reservoirs, and the interactions between them.

weak magnetic field B_{1I}. This situation corresponds to a large difference of spin populations between the abundant spin levels with $m_I = 1/2$ and $m_I = -1/2$, in other words to a very low spin temperature. This means that the I spin subsystem has, just before the CP contact, a high inverse spin temperature β_I^0. At this moment, the magnetization of the S spins in the rotating frame is zero, equivalent to an infinite spin temperature or zero inverse spin temperature β_S. The Hartmann−Hahn match, $\gamma_I B_{1I} = \gamma_S B_{1S}$, brings the subsystems to thermal contact, which enables the flow of energy and the concomitant polarization transfer to occur. As the system approaches thermodynamic equilibrium, the spin temperatures, and consequently inverse spin temperatures, tend to equalize. In other words, during cross-polarization the hot dilute spin subsystem S is cooled via thermal contact with the cool reservoir of the abundant spins I. At the same time, the subsystems I and S are also in contact with the lattice through the relaxation processes in the rotating frame, governed by the relaxation time constants $T_{1\rho}^I$ and $T_{1\rho}^S$, respectively. The overall process proceeds over a contact time t according to the following differential equations[1,7,8,11,18]

$$\frac{d\beta_S}{dt} = -(\beta_S - \beta_I)/T_{IS} - \beta_S/T_{1\rho}^S$$

$$\frac{d\beta_I}{dt} = -\epsilon\alpha^2(\beta_I - \beta_S)/T_{IS} - \beta_I/T_{1\rho}^I \quad (1)$$

The first terms on the right-hand-side of eq 1 describe CP, and the second terms are responsible for spin−lattice relaxation in the rotating frame. T_{IS} is a CP time constant, and its reciprocal, $1/T_{IS}$, is known as the CP rate constant. The remaining parameters are the spin population ratio $\epsilon = N_S/N_I$ and the Hartmann−Hahn matching coefficient $\alpha = \gamma_S B_{1S}/\gamma_I B_{1I}$. For the dilute-abundant spin system, ϵ is very small and at the exact Hartmann−Hahn match $\alpha = 1$. For the initial conditions discussed above

$$\beta_I(t = 0) = \beta_I^0 \text{ and } \beta_S(t = 0) = 0 \quad (2)$$

the general solution of eq 1 is

$$\beta_S(t) = \beta_I^0(a_+ - a_-)^{-1}[\exp(-a_- t/T_{IS}) - \exp(-a_+ t/T_{IS})] \quad (3)$$

where

$$a_\pm = c(1 \pm \sqrt{1 - d/c^2}) \quad (4)$$

$$d = (T_{IS}/T_{1\rho}^I)(1 + T_{IS}/T_{1\rho}^S) + \epsilon\alpha^2(T_{IS}/T_{1\rho}^S) \quad (5)$$

$$c = \frac{1}{2}(1 + \epsilon\alpha^2 + T_{IS}/T_{1\rho}^I + T_{IS}/T_{1\rho}^S) \quad (6)$$

Considering that the inverse spin temperatures are proportional to the respective magnetizations, which are in turn proportional to the peak intensities $I(t)$, we obtain the general CP equation of the form

$$I(t) = I_0(a_+ - a_-)^{-1}[\exp(-a_- t/T_{IS}) - \exp(-a_+ t/T_{IS})] \quad (7)$$

The absolute amplitude I_0 is in turn proportional to an equilibrium Bloch magnetization $M_{S,eq}$ in a typical one-pulse experiment without CP (the BD experiment), that is, to the amount of the sample

$$I_0 \propto M_{S,eq}\alpha(\gamma_I/\gamma_S) \quad (8)$$

Equation 7 is too complicated to be useful and has rarely been applied in practice.[17] When, for CP between the dilute and abundant nuclei, $\epsilon\alpha^2 \approx 0$, the general kinetic eq 7 reduces to

$$I(t) = I_0(1 + T_{IS}/T_{1\rho}^S - T_{IS}/T_{1\rho}^I)^{-1}\{\exp(-t/T_{1\rho}^I) - \exp[-t(1/T_{IS} + 1/T_{1\rho}^S)]\} \quad (9)$$

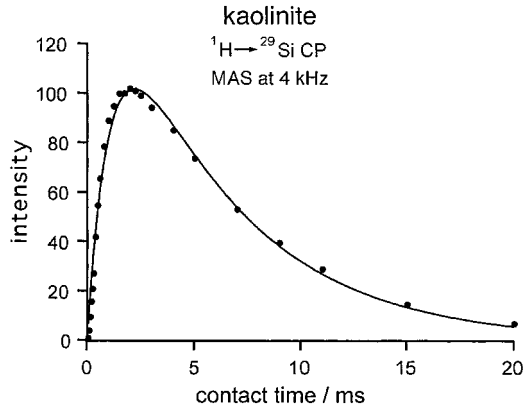

Figure 7. Typical classical CP kinetics using the example of kaolinite. Fitting using eq 10 gives $I_0 = 149 \pm 8$ (arbitrary units), $T^{I}_{1\rho} = 5.8 \pm 0.6$ ms, and $T_{IS} = 1.1 \pm 0.1$ ms.

When $\epsilon\alpha^2 \approx 0$ and $T_{IS}/T^{S}_{1\rho} \approx 0$, we can make a further simplification

$$I(t) = I_0(1 - T_{IS}/T^{I}_{1\rho})^{-1}[\exp(-t/T^{I}_{1\rho}) - \exp(-t/T_{IS})] \quad (10)$$

Finally, for the simplest kinetic case, $\epsilon\alpha^2 \approx 0$, $T_{IS}/T^{S}_{1\rho} \approx 0$, and $T_{IS}/T^{I}_{1\rho} \approx 0$, we have

$$I(t) = I_0[1 - \exp(-t/T_{IS})] \quad (11)$$

Equations 7, 9, and 10 describe the double-exponential behavior of CP intensity $I(t)$ versus contact time t (Figure 7). The intensity initially rises according to some time constant and then decreases according to another. A physical sense of the time constants depends on which equation is used. It is difficult to predict a priori which equation fits the experimental data best. Usually additional information on relaxation in the rotating frame is helpful in order to interpret a variable-contact-time experiment. Equation 9 differs from eq 10 in two respects: the CP time constant is $(1/T_{IS} + 1/T^{S}_{1\rho})^{-1}$ rather than T_{IS} and the preexponential factor contains the additional term $T_{IS}/T^{S}_{1\rho}$.[18] In consequence, the CP signal increases faster with contact time but its maximum value is reduced by the factor $(1 + T_{IS}/T^{S}_{1\rho} - T_{IS}/T^{I}_{1\rho})/(1 - T_{IS}/T^{I}_{1\rho})$ (Figure 8). Equation 7 has the effect of decreasing further both the apparent CP time constant and the maximum intensity. The simplest case corresponds to very slow spin−lattice relaxation in the rotating frame, and this gives an exponential increase with a time constant T_{IS}, reaching a plateau corresponding to the amplitude I_0. This case is the easiest to fit (cf. β-carotene in Figure 9 and the corresponding plots in Figure 10).[19]

Figure 10 illustrates several important problems. Note that the CP rates are different for different peaks, so a comparison of peak intensities on the basis of one particular spectrum, recorded with some arbitrarily chosen contact time, is meaningless. This point has already been raised in connection with Figure 3. In variable-contact-time experiments we can monitor peak amplitudes (Figure 10) or peak areas. The latter choice is preferable but less common in practice, since it requires spectral integration. The former choice is the right one if the shape of the peak is independent of contact time and one does not wish to compare the relative intensities of different peaks. The dependence of the peak shape on contact time would mean that the peak under consideration consists of several components which have different line widths and cross-polarize at different rates. This is reflected in the experimental kinetic curves and used for spectral assignment or in structural studies.

The peaks within the same CP spectrum must be compared on the basis of the absolute intensities I_0 obtained from fittings of the kinetic results. Quantitative comparison of different samples on the basis of their CP spectra is even more difficult. The situation in Figure 10 is very clear, because the values of I_0 correspond to the plateau levels. Note that even in this case some questions must be

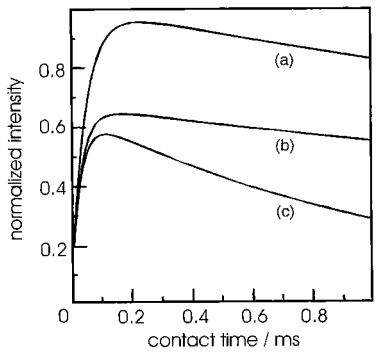

Figure 8. Simulated contact time curves: (a) curve based on eq 10 with $T_{IS} = 0.050$ ms, $T^{I}_{1\rho} = 5.0$ ms; (b) curve based on eq 9 with $T^{S}_{1\rho} = 0.10$ ms and the same values of T_{IS} and $T^{I}_{1\rho}$; (c) curve based on eq 7 with $\epsilon\alpha^2 = 0.10$ and the same values of T_{IS}, $T^{I}_{1\rho}$ and $T^{S}_{1\rho}$. Adapted, by permission, from ref 18.

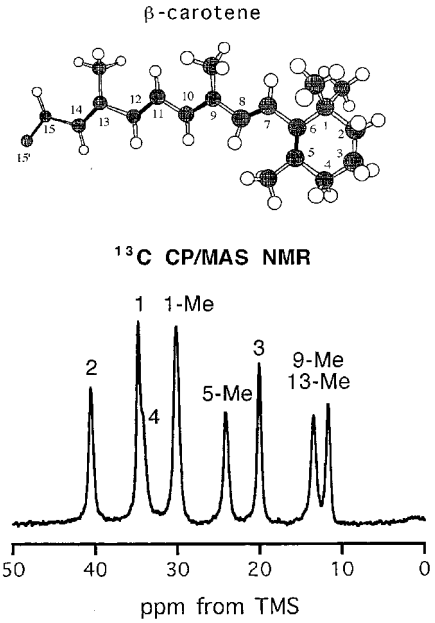

Figure 9. Structure of *trans*-β-carotene and the low-frequency part of its ^{13}C CP/MAS spectrum.[19] Black bars designate double C=C bonds. The molecule has a point of symmetry in the middle of the C15−C15′ bond. For clarity, the symmetry-related molecular segment has been omitted. The spectrum was recorded under MAS at 7 kHz with a 2.5 ms contact time.

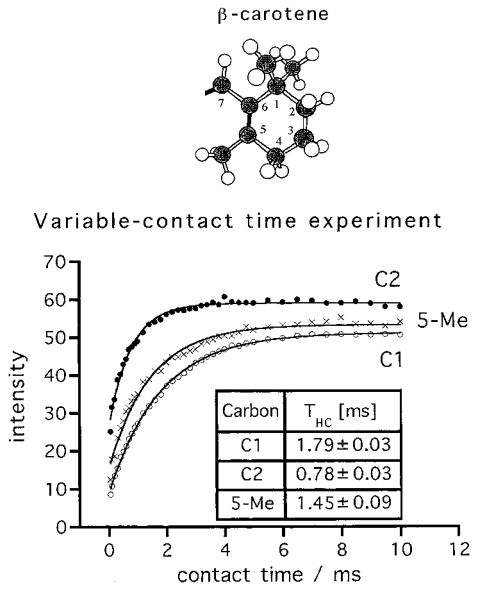

Figure 10. Selected kinetic CP curves for *trans-β*-carotene.[19]

addressed. Since for β-carotene the amplitudes were monitored and the line widths of the peaks were different, the plateau levels were also different, although for single carbon atoms they should be the same.

The CP time constants T_{IS} are characteristic of specific functional groups, since they are governed by dipolar interactions between the source spins I and the target spins S. The dipolar interaction has a $1/r^3$ dependence on the internuclear distance r, so that in general T_{IS} depends on the number of the nuclei involved in CP and on their disposition. The CP rate constant $1/T_{HC}$ (Figure 10) depends on the number of protons in a functional group and on the mobility of the group. The larger the number of protons in the group, the stronger the I−S dipolar interaction and the faster the cross-polarization. This is why the C2 carbon of the CH_2 group cross-polarizes faster than the quaternary carbon C1. Methyl carbons cross-polarize slowly, because a rapid group rotation about the ternary axis reduces dipolar interactions between its component spins. Methyl groups and CH groups usually have similar CP kinetics. Molecular motion also slows down CP, as explained in the context of cross-polarization in toluene/C_{70} (Figures 2 and 3).

For a rigid lattice, the CP rate constant has been expressed as[1,8,20]

$$\frac{1}{T_{IS}} = \frac{3}{2}\sqrt{\frac{2\pi}{5}}\frac{M_{2,IS}}{\sqrt{M_{2,II}}} \qquad (12)$$

where $M_{2,IS}$ and $M_{2,II}$ are the second moments,[21] which reflect the strength of the I−S and I−I dipolar interactions, respectively. Equation 12 tells us that for a rigid lattice CP proceeds faster when the heteronuclear dipolar interactions are strong and the homonuclear dipolar interactions between abundant spins are weak.

CP becomes less efficient when the second moments are reduced by molecular or group motions and

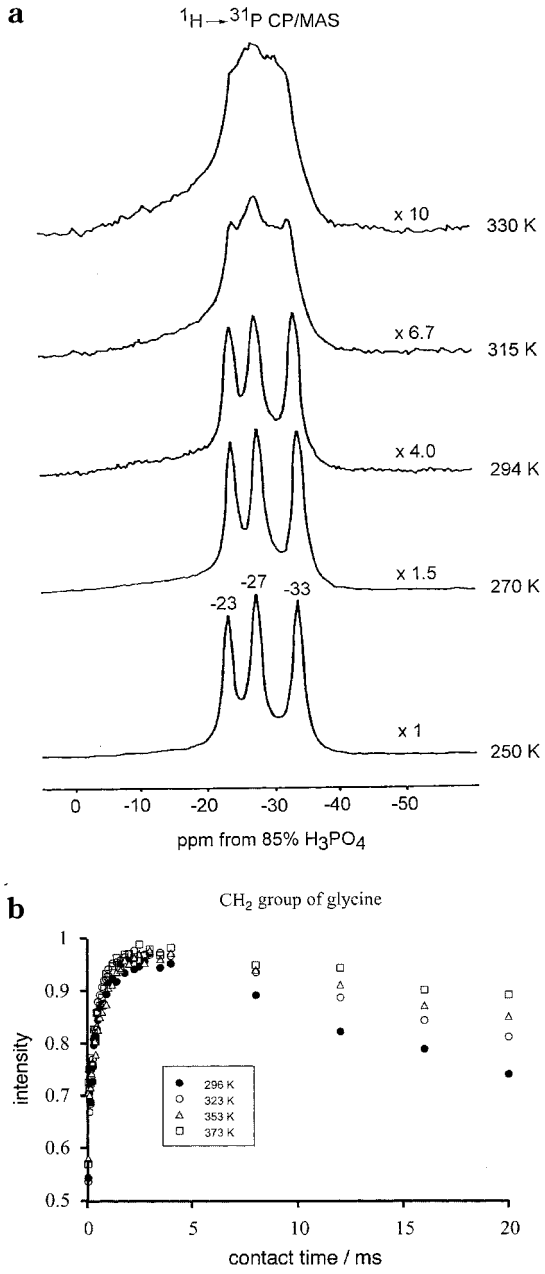

Figure 11. **(a)** Variable-temperature $^1H \rightarrow {}^{31}P$ CP/MAS NMR spectra of hydrated VPI-5 recorded under MAS at 8 kHz with a 5 ms contact time.[22] Note the different vertical expansion factors. The resonances at −23 and −27 ppm are due to P atoms in the 6−4 sites and the line at −33 ppm to P atoms in the 4−4 sites.[22,23] **(b)** Temperature dependence of the $^1H-{}^{13}C$ CP kinetics in glycine recorded with MAS at 7.5 kHz; the ^1H and ^{13}C frequencies were 400 and 100 MHz, respectively.

by MAS. Figures 11a and 12 illustrate the effects of the temperature and MAS rate on the CP efficiency in a porous aluminophosphate VPI-5.[22,23] Fast MAS differentiates CP rates for ^{13}C in solid organics, because it interferes with dipolar interactions and this can sometimes be used for peak assignment (Figure 13).[24] In the case of VPI-5, the ^{31}P nuclei cross-polarize from the protons of water. The water molecules gain considerable mobility with the temperature rise, so the $^1H-{}^{31}P$ CP intensity decreases very spectacularly (Figure 11a). On the other hand, in glycine the $^1H-{}^{13}C$ CP intensity for the optimum contact time is hardly affected by temperature,

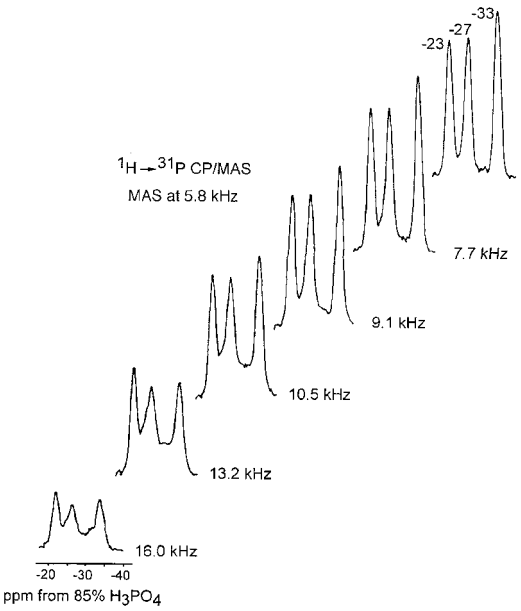

Figure 12. Influence of the rate of MAS on the ^{31}P CP spectrum of VPI-5, recorded with a 5 ms contact time.[23]

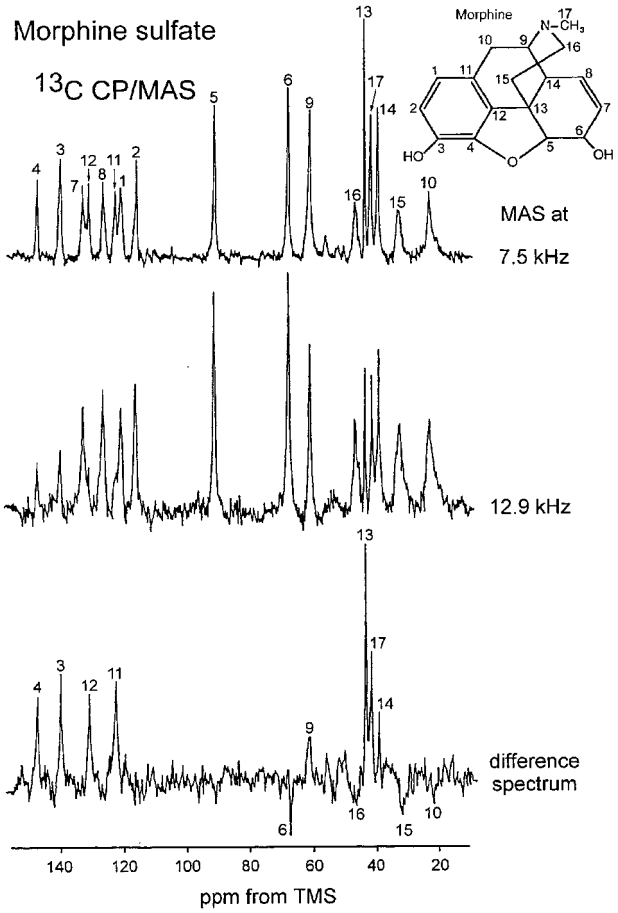

Figure 13. ^{13}C CP/MAS spectra of powdered morphine sulfate recorded with a contact time of 1 ms and recycle delay of 5 s (Bruker MSL-400). The spectra at the two MAS rates are not plotted on the absolute intensity scale. The difference spectrum (bottom) was obtained by subtracting the middle spectrum from the top spectrum after scaling the lines from CH aromatic carbons in both spectra to the same intensity.[24]

because the mobility of the molecular fragments in the crystal is less dependent on temperature (Figure 11b). The correlation time τ_c of the molecular motion decreases with faster motion, which in turn reduces the CP rate. A full theoretical approach to the problem requires that the dipolar correlation time τ_d also be taken into account. Depending on the magnitude of the τ_d/τ_c ratio, we can distinguish three motional regimes: (a) slow, with $\tau_d/\tau_c \leq 1$; (b) intermediate, with $\tau_d/\tau_c > 1$; (c) fast, with $\tau_d/\tau_c \gg 1$. In the slow motion regime, motion affects only $M_{2,II}$ and the function $1/T_{IS} = f(\tau_c)$ is nonlinear.[20] In the intermediate regime, both second moments are affected by the motion and the relationship between the motional (m) and rigid lattice (r) CP rate constants is very simple[20]

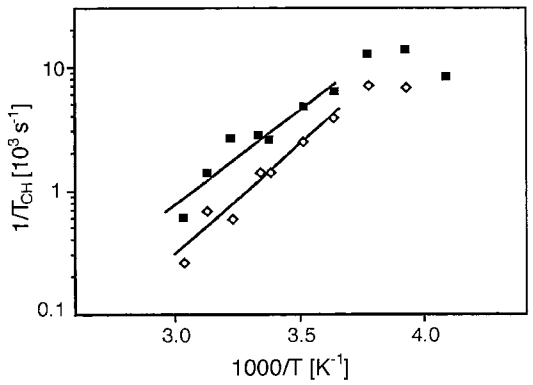

Figure 14. ^{1}H → ^{13}C CP rate versus the inverse temperature, using the spin-locking procedure under the Hartmann−Hahn match for a sample of elastomer with medium cross-link density. The data for CH_2 (■) and CH (◊) groups are shown together with the fitted lines. (Adapted with permission from ref 20.)

$$\frac{1}{T_{IS}^{(m)}} = \frac{2}{\pi}\frac{1}{T_{IS}^{(r)}}\tau_c \qquad (13)$$

The qualitative usefulness of eq 13 was verified by variable-temperature CP studies of polymers (Figure 14). The fast motion regime requires a special theoretical treatment,[25,26] which also predicts a double-exponential dependence of the CP intensity on the contact time, such as that in Figure 7. However, the relevant time constants have different physical meanings from those in eq 7. The fast motion case is relevant for cross-polarization involving highly mobile species, for example, molecules adsorbed at solid surfaces or fullerenes.[16]

According to eq 7, 9, and 10, the CP kinetics is not only determined by T_{IS}, but also by the relaxation times $T_{1\rho}^I$ and $T_{1\rho}^S$. For efficient CP, the latter relaxation times must be much longer than T_{IS}. Thus, for paramagnetic or conducting materials CP is difficult if not impossible. In favorable cases, $T_{IS} < 2$ ms and the range of $T_{1\rho}^I$ and $T_{1\rho}^S$ stretches from several miliseconds to infinity. Accordingly, the optimal CP contact times are typically in the 0.5−5 ms range. While T_{IS} and $T_{1\rho}^S$ characterize the individual chemical and/or crystallographic sites in a solid, the $T_{1\rho}^I$ of the protons is a volume property averaged over a distance of ca. 2 nm.[27] This provides the chemist with a tool for the study of heterogeneous solids. With very

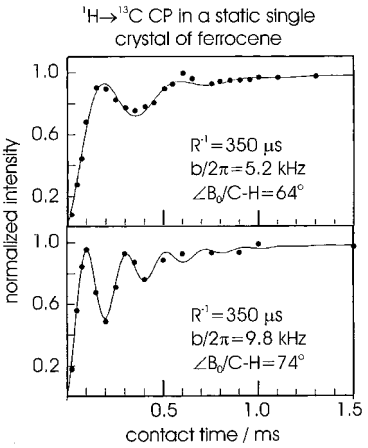

Figure 15. Oscillatory kinetics of ^{1}H → ^{13}C CP for the ferrocene lines from a static single crystal. (Adapted with permission from ref 31.)

heterogeneous samples it might be necessary to use "stretched exponentials" in order to account for the distribution of relaxation times[28] or CP rates.[29] A good discussion of rotating-frame relaxation in the context of CP is given in ref 30.

2.3. I–I*–S Model

Müller et al.[31] and Hester et al.[32] studied ^{1}H → ^{13}C CP in stationary single crystals of ferrocene and ammonium tartrate, respectively. They found that CP in the C−H bonds proceeds through transient harmonic oscillations, the frequency ω_{osc} of which depends on the orientation of the crystal in the external magnetic field (Figure 15), and it is equal to one-half of the dipolar splitting, *b*, of the peak from undecoupled ^{13}C spins. It appeared that magnetization shuttles between an isolated pair of ^{1}H and ^{13}C spins, mimicking the energy exchange between a pair of coupled pendulums. With time, the oscillations are gradually damped by the proton spin diffusion, which allows local protons directly involved in CP to exchange energy with the bulk protons. Spin diffusion relies on homonuclear dipolar interactions and proceeds through flip-flop spin transitions.[9,33] By contrast, the classical CP theory assumes that spin diffusion is sufficiently rapid to establish communication between the protons and to force them to behave as a single spin system at a uniform spin temperature, acting as the source of polarization. However, the proton spin-diffusion rate *R* is not sufficiently fast to prevent the oscillatory CP transfer observed in stationary single crystals of ferrocene and ammonium tartrate.[31,32] Müller et al.[31] described damped CP intensity oscillation for an isolated pair of spins 1/2 over a contact time *t* with the equation

$$I(t) = I_0\left[1 - \frac{1}{2}\exp(-Rt) - \frac{1}{2}\exp(-3Rt/2)\cos(bt/2)\right] \quad (14)$$

The method can be used for measuring heteronuclear dipolar couplings in stationary single crystals by one- and two-dimensional NMR which, in turn, allow the determination of molecular orientations and interatomic distances in solids.[13,34] Equation 14 was modified by Naito and McDowell[35] to include the

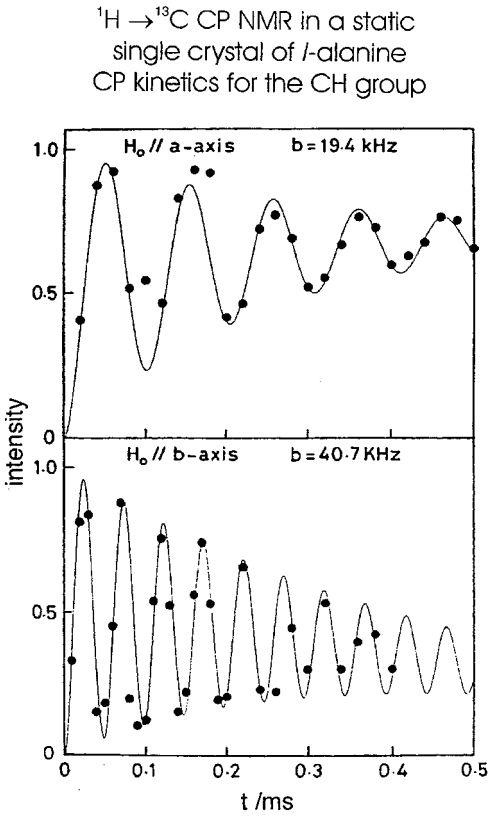

Figure 16. Oscillatory kinetics of ^{1}H → ^{13}C CP for the C_α carbon nucleus in a static single crystal of L-alanine. The curves were fitted with eq 15: R_I^z = 3400 s^{-1}, $R_I + R_S$ = 2000 s^{-1}, $T_{1\rho}^I$ = 3 ms and $T_{1\rho}^S$ = 21.6 ms for the upper graph, and R_I^z = 2000 s^{-1}, $R_I + R_S$ = 1300 s^{-1}, $T_{1\rho}^I$ = 0.6 ms, and $T_{1\rho}^S$ = 21.6 ms for the lower graph. (Adapted with permission from ref 35.)

effect of rare spin diffusion at a rate R_s and the effects of rotating-frame spin−lattice relaxation for spins I and S at rates $1/T_{1\rho}^I$ and $1/T_{1\rho}^S$, respectively

$$I(t) = I_0\left\{\left(\frac{1}{2} - \frac{R_I + R_S}{R_I + R_S + 1/T_{1\rho}^S}\right)\exp[-(R_I + R_S + 1/T_{1\rho}^S + 1/T_{1\rho}^I)t] + \frac{R_I + R_S}{R_I + R_S + 1/T_{1\rho}^S}\exp(-t/T_{1\rho}^I) - \frac{1}{2}\exp[-(R_I^z + 2R_I + 2R_S - 1/T_{1\rho}^S + 1/T_{1\rho}^I)t/2]\cos(bt/2)\right\} \quad (15)$$

R_I^z and R_I are rates of proton spin-diffusion, and this varies with the proton decoupling power and crystal orientation.[36] Equation 15 was verified experimentally on a stationary single crystal of L-alanine (Figure 16).[35] For very slowly relaxing dilute spins S and for isotropic proton spin diffusion, $T_{1\rho}^S = \infty$, $R_S = 0$, $R_I^z = R_I = R$, and eq 15 yields

$$I(t) = I_0\exp(-t/T_{1\rho}^I)\left\{1 - \frac{1}{2}\exp(-Rt) - \frac{1}{2}\exp[-(3R - 1/T_{1\rho}^I)t/2]\cos(bt/2)\right\} \quad (16)$$

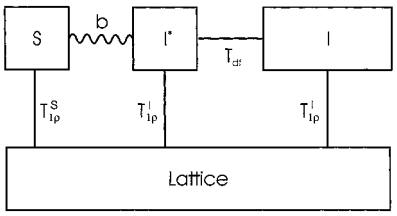

Figure 17. Block diagram of I−I*−S CP thermodynamics.

Since $3R \gg 1/T_{1\rho}^{I}$, eq 16 simplifies further to

$$I(t) = I_0 \exp(-t/T_{1\rho}^{I})\left[1 - \frac{1}{2}\exp(-t/T_{df}) - \frac{1}{2}\exp\left(-\frac{3}{2}t/T_{df}\right)\cos(bt/2)\right] \quad (17)$$

where we have introduced the proton spin-diffusion constant $T_{df} = 1/R$. For $T_{1\rho}^{I} = \infty$, eq 17 reduces to eq 14.

To summarize, the authors of refs 31−36 and Levitt et al.[37] proposed a new model of cross-polarization, often known as the I−I*−S model, where the asterisk denotes protons in close proximity to the S nucleus (or S nuclei). Within this model, source spins, such as protons, do not have a common spin temperature. The I*−S spin pairs or clusters can be viewed as isolated in a solid and exchanging polarization in an oscillatory manner, damped by the subsequent spin-diffusion contact with the remaining I spins. The kinetics of CP according to this model is described by eqs 14−17. Figure 17 shows the thermodynamic scheme for the I−I*−S model, with the principal interactions in the system and the time constants describing the relevant energy transfers. The model was verified on stationary single crystals.

In 1988, Wu et al.[38] found that for CH and CH_2 groups $^1H \rightarrow {}^{13}C$ CP under MAS in polycrystalline organic compounds proceeds in two stages. By contrast, for quaternary carbons and CH_3 groups, both subject to weak heteronuclear dipolar interactions, polarization transfer can be rationalized in terms of the classical CP theory. Anxious to avoid the effects of proton spin−lattice relaxation in the rotating frame, Wu et al.[38] studied cross-depolarization (CD) of ^{13}C rather than CP (Figure 18). For the CH and CH_2 groups in polycrystalline terephthalic acid and glycine, respectively, the experiments revealed the presence of very rapid depolarization during the first tens of microseconds, followed by much slower depolarization reaching a plateau within ca. 1 ms (Figure 19). The explanation was based on the arguments used for stationary single crystals. The first depolarization stage was explained by a fast energy exchange between the ^1H and ^{13}C spins in the CH and CH_2 groups and the second stage by a spin-diffusion contact of directly bound protons with the remaining protons.

For clarity, before discussing the kinetic functions of CD in rotating powders, it is necessary to see what happens in a static powder. Consider a static powdered sample containing equivalent carbon atoms in the CH groups (carbons with the same chemical shift tensor). The sample gives a NMR powder pattern, every point of which corresponds to a different

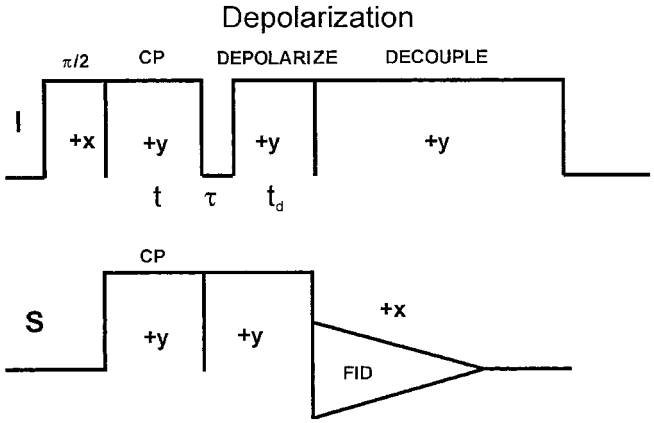

Figure 18. Depolarizing pulse sequence. After initial CP over a contact time t, B_{1I} is turned off and the I magnetization disappears due to spin−spin relaxation over a time period τ, while the S magnetization is still locked along B_{1S}. Then B_{1I} is turned on again and the S magnetization depolarizes over a variable time period t_d. (Adapted with permission from ref 38.)

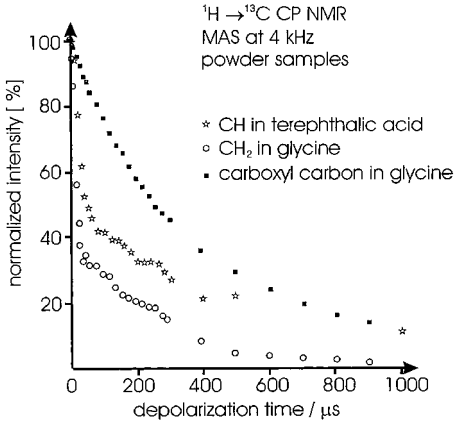

Figure 19. I−I*−S depolarization kinetics for rotating powders with the characteristic two-stage behavior of protonated carbons. (Adapted with permission from ref 38.)

orientation of the C−H bonds with respect to the external magnetic field, and hence to a certain dipolar coupling b. In principle, for very slow rotating-frame relaxation of protons, CD should be an exact reciprocal process to CP. Each point in a static powder pattern should therefore show an oscillatory magnetization transfer according to eq 14 as modified for the CD case to give

$$I(t) = I_0\left[\frac{1}{2}\exp(-t/T_{df}) + \frac{1}{2}\exp\left(-\frac{3}{2}t/T_{df}\right)\cos(bt/2)\right] \quad (18)$$

This behavior was demonstrated using a static powdered sample of ferrocene.[39]

When a sample contains several types of carbon atoms, the different powder patterns overlap and a particular spectral point will simultaneously belong to several different powder patterns. It follows that the point will oscillate with several different frequences and the oscillations will interfere. In highly heterogeneous powder samples the oscillations will mutually cancel out and the CD or CP kinetic curves will appear virtually smooth even without sample spinning.

Return to the case of a single powder pattern and assume that the sample begins to rotate. The contributions from all the magnetically equivalent S spins in the molecules with different orientations will then be added to form a single narrow line or a center band flanked by sidebands.[40] The oscillations with different frequencies will destructively interfere with each other, resulting in rapid exponential CP or CD.[38]

To quantify this behavior, we need to calculate the mean value of $\cos(bt/2)$ over all orientations of the crystallites. We follow the procedure proposed by Alemany et al.[41]

$$\overline{\cos(b_i t/2)} = \frac{\sum_i I_i \cos(b_i t/2)}{\sum_i I_i} = \frac{\sum_i I_i \left[1 - \frac{(b_i t/2)^2}{2!} + \frac{(b_i t/2)^4}{4!} - \cdots\right]}{\sum_i I_i} \quad (19)$$

For very short contact times, the higher terms in the expansion vanish and

$$\overline{\cos(b_i t/2)} \cong 1 - \left[\frac{\sum_i I_i (b_i/2)^2}{\sum_i I_i}\right]\frac{t^2}{2!} \quad (20)$$

Substituting

$$\frac{\sum_i I_i (b_i/2)^2}{\sum_i I_i} = \frac{1}{{T_2}^2} \quad (21)$$

we have

$$\overline{\cos(b_i t/2)} \cong 1 - \frac{t^2}{2!{T_2}^2} \cong \exp(-t^2/2{T_2}^2) \quad (22)$$

Instead of oscillations, there will be a rapid Gaussian decay of the S magnetization at the very begining of the CD kinetic curve. The decay rate $1/T_2$ may be considered as a root-mean-squared average of $b_i/2$ properly weighted by the fraction $I_i/\sum_i I_i$ of molecules with a given orientation corresponding to the oscillation frequency $b_i/2$.[41] The resulting equations for the CH group are

$$\text{CD} \quad I(t) = I_0\left[\frac{1}{2}\exp(-t/T_{\text{df}}) + \frac{1}{2}\exp\left(-\frac{3}{2}t/T_{\text{df}}\right)\exp\left(-\frac{1}{2}t^2/{T_2}^2\right)\right] \quad (23)$$

$$\text{CP} \quad I(t) = I_0\left[1 - \frac{1}{2}\exp(-t/T_{\text{df}}) - \frac{1}{2}\exp\left(-\frac{3}{2}t/T_{\text{df}}\right)\exp\left(-\frac{1}{2}t^2/{T_2}^2\right)\right] \quad (24)$$

Note that the initial very fast depolarization removes one-half of the CP intensity of the signal of the CH group (Figure 19). This is in accordance with eq 23, where the last term in brackets accounts for the sudden intensity loss and has a preexponential factor of 1/2. The second half of the CP intensity decays slowly according to the exponential governed by proton spin-diffusion (the first term in the brackets in eq 23, also preceded by the factor of 1/2).

For the CH_2 group, the initial very fast depolarization removes 2/3 of the CP intensity and the final slow depolarization removes the remaining 1/3 (Figure 19). Under the Hartmann−Hahn match, the S spin has the same rotating-frame energy splitting as the I spin, and after reaching equilibrium, the three spins (one S spin and two I spins) will share equally the Zeeman energy offered by the S spin.[38,42] The resulting equations for the CH_2 group are[38]

$$\text{CD} \quad I(t) = I_0\left[\frac{1}{3}\exp(-t/T_{\text{df}}) + \frac{2}{3}\exp\left(-\frac{3}{2}t/T_{\text{df}}\right)\exp\left(-\frac{1}{2}t^2/{T_2}^2\right)\right] \quad (25)$$

$$\text{CP} \quad I(t) = I_0\left[1 - \frac{1}{3}\exp(-t/T_{\text{df}}) - \frac{2}{3}\exp\left(-\frac{3}{2}t/T_{\text{df}}\right)\exp\left(-\frac{1}{2}t^2/{T_2}^2\right)\right] \quad (26)$$

In general, for isolated SI_n clusters in a powder sample under MAS but without extensive molecular motion, one would expect the following to hold

$$\text{CD} \quad I(t) = I_0\left[\lambda\exp(-t/T_{\text{df}}) + (1-\lambda)\exp\left(-\frac{3}{2}t/T_{\text{df}}\right)\exp\left(-\frac{1}{2}t^2/{T_2}^2\right)\right] \quad (27)$$

$$\text{CP} \quad I(t) = I_0\exp(-t/T_{1\rho}^{\text{I}})\left[1 - \lambda\exp(-t/T_{\text{df}}) - (1-\lambda)\exp\left(-\frac{3}{2}t/T_{\text{df}}\right)\exp\left(-\frac{1}{2}t^2/{T_2}^2\right)\right] \quad (28)$$

where the rotating-frame relaxation is assumed for protons during CP and $\lambda = 1/(n+1)$.

3. Applicability of the Two Models of Cross-Polarization

It is not possible to predict in advance which of the two models will best describe any particular kinetic CP results. However, we shall give the reader a feeling as to what could be expected. Consider the work of Tian and Cross who studied $^1H \rightarrow {}^{15}N$ CP in ^{15}N-labeled gramicidin A oriented in a hydrated lipid bilayer (Figure 20).[43] In the protonated sample they observed damped dipolar oscillations, typical for the kinetic I−I*−S model. The results were fitted using eq 17. The sample was then deuterated, so that the protons at nitrogen atoms were substituted by deu-

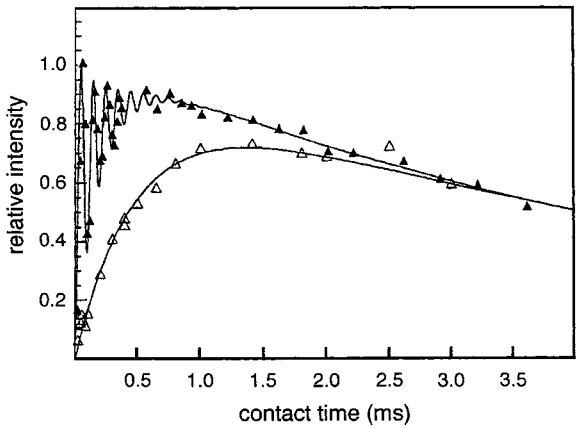

Figure 20. $^{1}H \rightarrow {}^{15}N$ CP kinetics in ^{15}N-labeled gramicidin A oriented in a hydrated lipid bilayer. The original sample (▲) shows dipolar oscillations in accordance with eq 17 of the I−I*−S model: $T_{df} = 280\ \mu s$, $T_{1\rho}^{H} = 5.4$ ms, $b = 20$ kHz. The deuterated sample (△) behaves according to eq 10 of the I−S model: $T_{HN} = 500\ \mu s$, $T_{1\rho}^{H} = 5.4$ ms. (Adapted with permission from ref 43.)

terons but the nonsubstituted protons in the aliphatic groups still retained substantial homonuclear dipolar coupling. Thus, nitrogen-15 was forced to cross-polarize from a remote proton pool via weak heteronuclear dipolar interactions. Upon deuteration, the CP kinetics complies with the classical I−S model and the fitting used eq 10. It turns out that, in principle, the kinetic I−I*−S model applies when the heteronuclear I*−S dipolar interactions are sufficiently strong compared with the homonuclear I−I dipolar interactions. This is the case when the nuclei involved in CP are close in space, as, for example, ^{1}H and ^{13}C in the same functional group, and if such groups are relatively immobile. For weak I−S heteronuclear dipolar interactions and moderate or strong I−I homonuclear dipolar interactions, the CP kinetics is likely to follow the classical model.

Chemists are mostly interested in $^{1}H \rightarrow {}^{13}C$ CP/MAS spectra. In the presence of substantial segmental chain motion, molecules such as β-carotene[19] (Figure 10) and polymers[20,30] comply with the classical kinetic model. In less mobile organic molecules, CP proceeds according to the I−I*−S model for the CH and CH_2 groups. It is usually assumed that quaternary carbons and fast rotating methyl groups cross-polarize according to the classical I−S model, but this is not necessarily correct. Consider an example from supramolecular chemistry: $^{1}H \rightarrow {}^{13}C$ CP/MAS NMR in resorcinarene (Figure 21a). All the resorcinarene carbons including quaternary carbons and carbons in the terminal methyl groups cross-polarize according to the I−I*−S model (Table 1, Figure 21). By contrast, the DMF molecules introduced into the resorcinarene crystal lattice cross-polarize according to the classical I−S model (Figure 22).[44] Thus, both CP kinetic models can meet in the same composite material, in the sense that different molecular components or phases cross-polarize according to different kinetic models.

Note that in theory the value of λ is 1/2 and 1/3 for the CH and CH_2 groups,[38,42] respectively. In practice

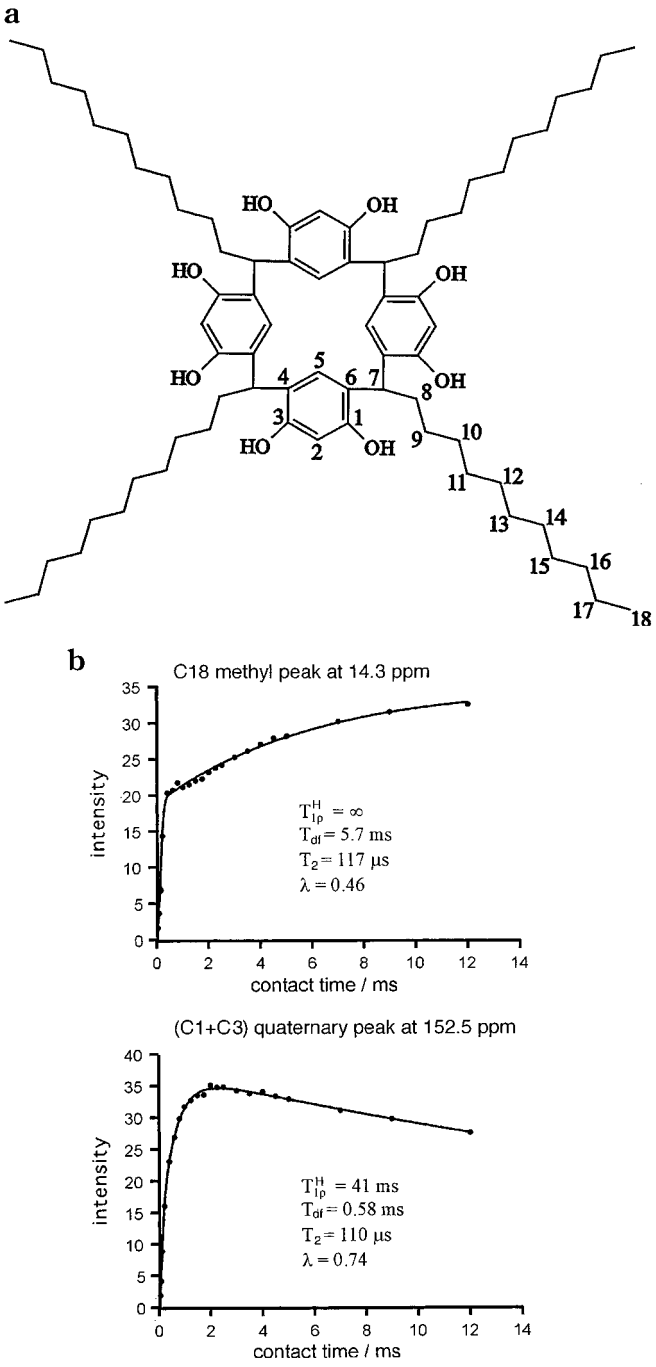

Figure 21. Tetra(*C*-undecyl)calix[4]resorcinarene and its derivatives are potential complexing agents for chromatographic and pharmaceutical applications. The crystallographic structure of the pure compound has not been determined, because the crystals are not suitable for single-crystal X-ray diffraction. It is likely that the aromatic rings form a calix, such as that in the resorcinarene/DMF complex.[44] The compound is a good candidate for $^{1}H \rightarrow {}^{13}C$ CP/MAS NMR studies (at 200 and 50 MHz for ^{1}H and ^{13}C, respectively; MAS at 4.5 kHz). All the carbons cross-polarize according to the I−I*−S model. Two fittings using eq 28 are shown.

it is not so, and our experience indicates that λ and the other CP kinetic parameters depend on group mobility. Therefore, λ must be fitted for those groups and also for the quaternary carbons and methyl groups if they comply with the I −I*−S model (Figure 21). To broaden the range of kinetic results, we consider the $^{1}H \rightarrow {}^{13}C$ CP/MAS NMR in a genistein/

Table 1. $^1H \rightarrow {}^{13}C$ CP NMR Parameters for Selected Groups in Resorcinarene and in the Genistein/Piperazine Complex (at 50 MHz for ^{13}C, MAS at 4.5 KHz), Cross-Polarizing According to the I−I*−S Model[a]

group	assignment	$T_{1\rho}^H$[ms]	T_{df} [ms]	T_2 [μs]	λ
		resorcinarene			
quaternary	C1,C3	41 ± 2	0.58 ± 0.03	110 ± 10	0.74 ± 0.03
quaternary	C1,C3	44 ± 3	0.63 ± 0.04	72 ± 7	0.75 ± 0.02
CH	C2	35 ± 2	0.42 ± 0.02	15 ± 1	0.48 ± 0.02
CH	C7	40 ± 3	0.22 ± 0.02	19 ± 1	0.45 ± 0.03
CH_2	C8	∞	0.41 ± 0.05	33 ± 2	0.41 ± 0.03
CH_2	C17	∞	3.8 ± 0.4	81 ± 3	0.43 ± 0.01
CH_3	C18	∞	5.7 ± 0.9	117 ± 5	0.46 ± 0.02
CH_3	C18	∞	2.0 ± 0.2	76 ± 8	0.61 ± 0.02
		genistein/piperazine complex			
quaternary	genistein	62 ± 4	0.93 ± 0.04	117 ± 8	0.72 ± 0.02
CH	genistein	63 ± 4	0.48 ± 0.04	not determined	0.41 ± 0.02
CH_2	piperazine	55 ± 4	0.30 ± 0.05	not determined	0.31 ± 0.02

[a] In the crystal structure of resorcinarene, functional groups of the same kind are located in inequivalent positions. For the genistein/piperazine complex we give mean values for all the groups of the same kind.

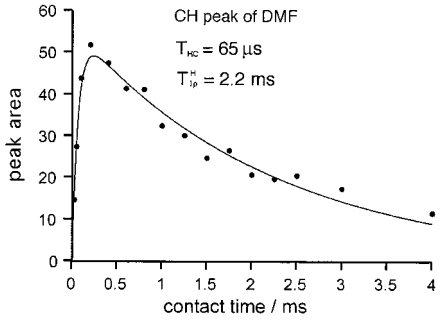

Figure 22. $^1H \rightarrow {}^{13}C$ CP kinetics for DMF in the resorcinarene/DMF complex (at 200 and 50 MHz for ^1H and ^{13}C, respectively; MAS at 4.5 kHz).[44] The fitting uses eq 10 of the I−S model.

piperazine complex, a substance of medical interest (Table 1 and Figure 23).[45] In this case, the fitting for the nonquaternary carbons used the simplified eq 29

$$I(t) = I_0 \exp(-t/T_{1\rho}^H)[1 - \lambda \exp(-t/T_{df})] \quad (29)$$

derived from eq 28 by putting $T_2 = 0$. This simplified approach, valid for very short T_2, allows one to dispense with the rather inaccurate determination of T_2 and to assess easily $T_{1\rho}^H$, T_{df}, and λ. The results in Table 1 show that the values of $T_{1\rho}^H$ for the resorcinarene calix and for the C_{11} aliphatic chains are different. We believe that this is caused by the higher mobility of the aliphatic chains than of the calix. The methyl groups are an exception, since they rotate very fast, and thus, all three time constants ($T_{1\rho}^H$, T_{df}, and T_2) are relatively long. As the proton spin-diffusion rates $1/T_{df}$ depend not only on the number of hydrogen atoms in a functional group but also on group mobility, they are not fully specific to the kind of group. For quaternary and methyl carbons the T_2 time constant is on the order of 0.1 ms but is usually considerably shorter for the other carbons. Fittings give $\lambda = 0.7-0.8$ for quaternary carbons, $\lambda = 0.4-0.6$ for the methyl carbons, and for the CH and CH_2 groups, λ deviates by not more than 0.1 from the theoretical values of 1/2 and 1/3, respectively. Accordingly, different ^{13}C CP rates for various functional groups were proposed for spectral

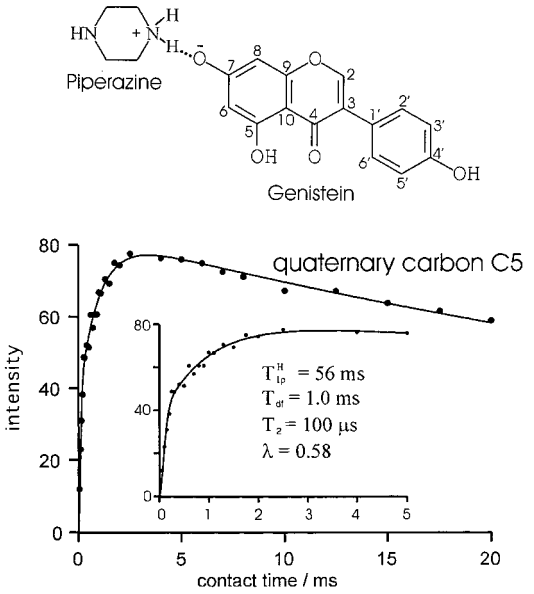

Figure 23. Genistein, 5,7-dihydroxy-3-(4′-hydroxyphenyl)-4*H*-chromen-4-one, is a natural isoflavone of medical interest, as many of its derivatives exhibit immunosuppressant activity. The $^1H \rightarrow {}^{13}C$ CP kinetics under MAS at 4.5 kHz in the genistein/piperazine complex follows eq 28 of the I−I*−S model.[45] The inset shows the expanded 0−5 ms region of the plot.

editing of CP/MAS spectra of organic compounds.[46−49] Our experience indicates that this should be done with caution. The results in Table 1 reveal the general trends and should by no means be considered typical. We believe that much further experimental work needs to be done before the ranges for T_{df}, T_2, and λ in particular carbon environments are properly established.

There are two simple special cases of the I−I*−S model. Either, in accordance with eq 17, strong oscillations are present or the CP kinetic curve is smooth in accordance with eq 28. These extreme cases are the easiest to interpret. However, one can also encounter residual oscillations, as in the case of $^1H \rightarrow {}^{31}P$ CP in powdered human bone under MAS (Figure 24),[50] or a sharp initial peak in CP intensity, as in the case of $^2H \rightarrow {}^1H$ CP in deuterated glycine under MAS (Figure 25).[51] Such kinetic behavior has

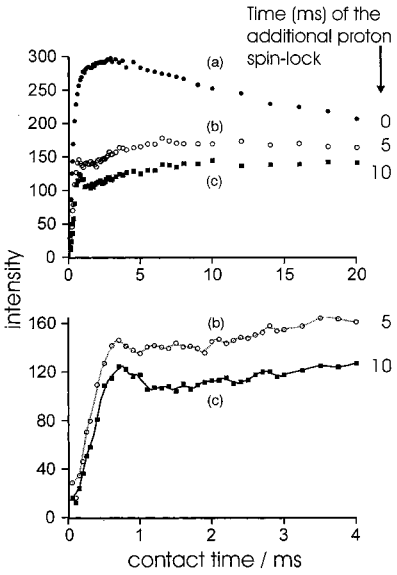

Figure 24. $^{1}H \rightarrow {}^{31}P$ CP kinetics under MAS at 3 kHz in powdered human trabecular bone.[50] This complex material gives only one structureless peak, and the CP kinetic studies shed some light on its composition. The curve (a) was measured by a conventional CP experiment. To eliminate from CP protons with a short relaxation time $T_{1\rho}^{H}$, the CP stage was preceded by an additional proton spin lock (curves b and c). The bottom curves, corresponding to an expanded short contact-time range, show dipolar oscillations.

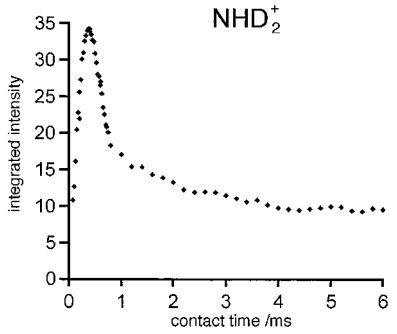

Figure 25. $^{2}H \rightarrow {}^{1}H$ CP kinetics in deuterated polycrystalline glycine under MAS at 5 kHz.[51] The sudden initial increase in intensity is often observed in spin systems cross-polarizing according to the I−I*−S model, but with markedly damped CP oscillations.

also been found by others. For example, residual oscillations were described by Walter et al.[18] for $^{1}H \rightarrow {}^{17}O$ CP in $Ca(OH)_2$, and the sharp initial CP maximum was observed by Hawkes et al.[52] for $^{1}H \rightarrow {}^{13}C$ CP with MAS in a hydrido osmium complex. In such intermediate cases, the best strategy is to exclude the contact-time period of residual oscillations from the fitting[42] or to apply eq 17 with substantial damping, i.e., to use a large value of T_{df}. In any case, the cited publications demonstrate that I−I*−S behavior can be found in various materials, even in liquid crystals,[53] also if quadrupolar nuclei are involved in CP both as source and target spins.

Although cross-polarization was designed for the enhancement of peaks from rare spins by the polarization transfer from abundant spins, it works quite well when both the source and the target spins are abundant. In this case, one is more interested in the

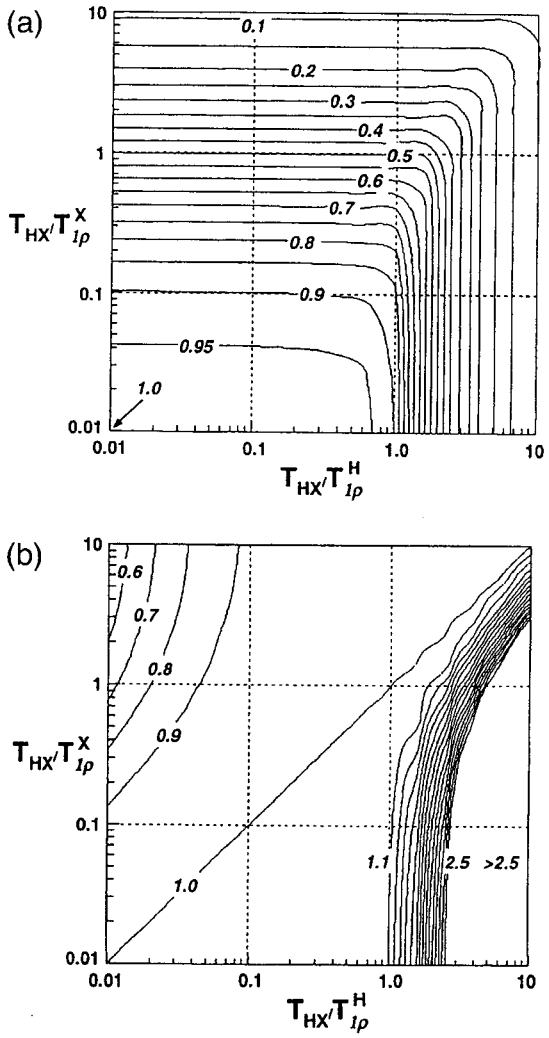

Figure 26. Contour maps of parameters (a) f_1 and (b) f_2 for the $^{1}H \rightarrow X$ CP according to the I−S model with $\epsilon = 0.01$, useful for $X \equiv {}^{13}C$ at natural abundance. (Adapted with permission from ref 54.)

structural information provided by the parameters of CP kinetics. The true abundant/abundant case can only be discussed in terms of the I−S model, since in this case isolated clusters containing I and S spins simply do not exist. The original eqs 4−7 of the I−S model are valid for both the rare/abundant (no isolated spin clusters, rare spins coupled to the abundant reservoir, spin temperature for rare spins exists) and abundant/abundant cases. In either case, the kinetic CP curve is double-exponential (eq 7) and the fitted time constants, $T_{IS}^{*} = T_{IS}/a_{+}$ and $T_{1\rho}^{*} = T_{IS}/a_{-}$, differ from those predicted by the reduced eq 10. Ando, Harris, and Reinsberg[54] introduced two convenient parameters, $f_1 = T_{IS}^{*}/T_{IS}$ and $f_2 = T_{1\rho}^{*}/T_{1\rho}^{I}$, and described a method of deriving them on the basis of variable-contact-time and "CP drain" experiments. Clearly, for the extreme situation when $\epsilon \ll 1$ and $T_{IS} \ll T_{1\rho}^{I} \ll T_{1\rho}^{S}$, we have $f_1 = 1$ and $f_2 = 1$. For $\epsilon = 0.01$ (^{13}C at natural abundance) and $\epsilon = 1$, one can use contour maps from ref 54 (Figure 26). The procedure proposed in that work is valid for the centerband matching of the Hartmann−Hahn condition.

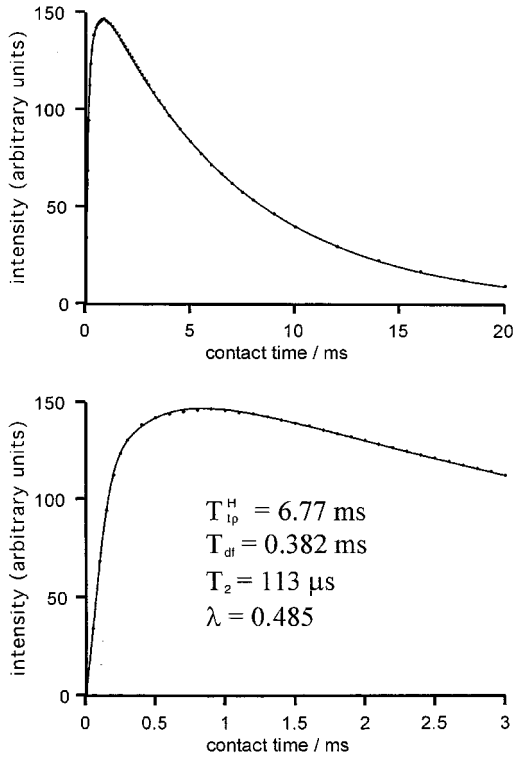

Figure 27. $^1H \rightarrow {}^{31}P$ CP kinetics under MAS at 3 kHz in natural polycrystalline brushite, $CaHPO_4 \cdot 2H_2O$, shown for full (above) and initial (below) contact time ranges.[55] The fitting uses eq 28 of the I−I*−S model.

4. Practical Considerations

To discriminate between the different CP kinetic models, the early part of the CP kinetic curve must be very accurately sampled. Only then is it possible to detect oscillations or a sudden initial rise of the CP signal, both characteristic of the I−I*−S model. At first glance, the CP kinetics sometimes seems to comply with the classical I−S model (two stages: rise and decay). However, after extending the initial contact-time range it becomes clear that CP proceeds in three stages (fast rise with possible oscillations, slow rise, and decay) according to the I−I*−S model. As an example, consider the $^1H \rightarrow {}^{31}P$ CP kinetic results for polycrystalline brushite, $CaHPO_4 \cdot 2H_2O$, obtained under MAS (Figure 27).[55]

The fitting using either model involves several parameters. To obtain an accurate fitting, one usually begins by determining some of the CP parameters using other independent experiments. The T_{IS}, T_2, T_{df}, and λ parameters can be obtained from depolarization (see below) or from TORQUE experiments[29] (Figure 28), while the relaxation parameters, $T^I_{1\rho}$ and $T^S_{1\rho}$, can be measured by means of CP sequences with extra variable spin-locking at the I or S channels (Figures 29 and 30), respectively.

The depolarization experiment (Figure 18) is useful for the determination of T_2 of the I−I*−S kinetics, because the initial depolarization period follows eq 27. However, for longer depolarization times, the CP intensity unexpectedly decays with a time constant $T^*_{1\rho} \approx T^H_{1\rho}$ (Figure 31). In practice, the depolarization curve can be fitted using eq 27, supplemented on its right-hand side with the term $A \exp(-t/T^*_{1\rho})$, where A is the amplitude. For a long depolarization time in a homogeneous material, when according to the I−I*−S model spins I* are already in contact with spins I via spin diffusion, the overall spin subsystem I achieves a common spin temperature. In this case, the CP kinetics proceeds according to the I−S model, so both kinetic models may meet in the same depo-

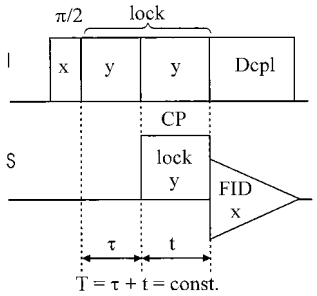

Figure 28. TORQUE pulse sequence,[29] using concerted variation of τ and t, but with their sum T = const.

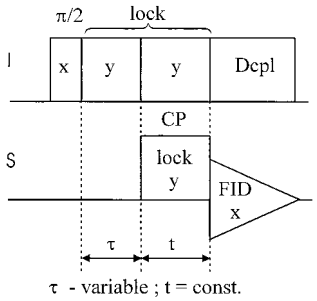

Figure 29. Pulse sequence for measuring the relaxation time $T^I_{1\rho}$ of the I nuclei.

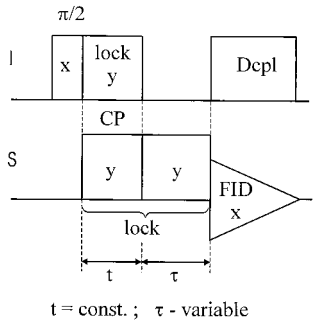

Figure 30. Pulse sequence for measuring the relaxation time $T^S_{1\rho}$ of the S nuclei.

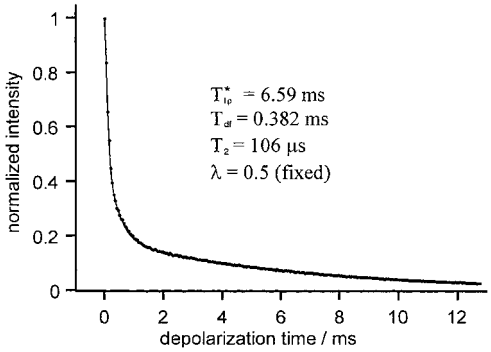

Figure 31. Depolarization curve for brushite fitted using eq 27 supplemented on its right-hand side with the term $A \exp(-t/T^*_{1\rho})$. Compare the fitted parameters with those given in Figure 27.

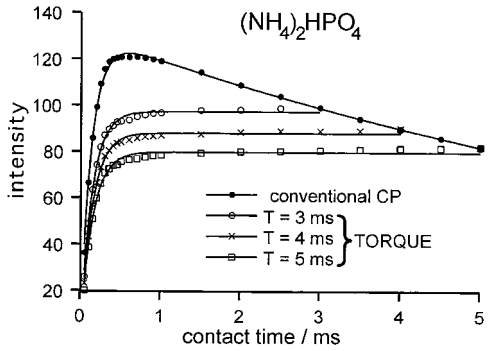

Figure 32. Comparison of conventional $^1H \rightarrow {}^{31}P$ CP and TORQUE kinetic curves for $(NH_4)_2HPO_4$. Note that there is no rotating-frame spin−lattice relaxation effect on the TORQUE curves. The results were analyzed according to the I−S model, using full eq 10 for conventional CP and eq 10 with $\exp(-t/T^I_{1\rho}) = 1$ and $T_{IS}/T^I_{1\rho} = 0$ for TORQUE. Conventional CP gives $T_{HP} = 134\ \mu$s, while TORQUE gives $T_{HP} = 142$ (○), 145 (×) and 149 μs (□).

larization curve. The depolarization kinetics for a long depolarization time can be rationalized using the classical CP model.[56]

The TORQUE experiment (T One Rho QUEnching) (Figure 28) uses a concerted variation of τ and t but with the overall proton lock period T being constant.[29] The CP curve is thus unaffected by relaxation in the rotating frame. It follows that for fitting the TORQUE results it is best to use eqs 10 and 28 with infinitely long $T^I_{1\rho}$, so that $T_{IS}/T^I_{1\rho} = 0$ and $\exp(-t/T^I_{1\rho}) = 1$. Examples are given in Figure 32.

Relaxation in the rotating frame can be studied by conventional variable-spin-lock experiments without using CP. However, the pulse programs shown in Figures 29 and 30 have the advantage of monitoring only the nuclei participating in CP. For homogeneous samples the results should be fitted with eq 30

$$I(\tau) = A \exp(-\tau/T_{1\rho}) \qquad (30)$$

while for heterogeneous samples one should try a multiexponential function.

The reader should be aware that there are other reasons for CP heterogeneity. Under a mismatched Hartmann−Hahn condition the rare S spins belong to several categories, each participating in CP with a different rate.[42] In some SI_n groups, this results in CP taking place on the scale of tens of microseconds while others polarize much more slowly. Correct setting of the Hartmann−Hahn condition is thus essential. One should be also aware of the rotational sidebands caused by MAS in the Hartmann−Hahn spectrum (intensity vs B_{1I} or B_{1S}).[57] When matched at first- or second-order sidebands, CP proceeds under fast MAS with strong dipolar oscillations.[58] Fourier transformation leads to Pake-like patterns, which provide information on internuclear distances.[58] Finally, we note that all the measurements discussed in this review rely on the stability of the B_{1I} and B_{1S} fields during the respective spin-lock periods. It is essential to confirm that the levels of the locking fields are strictly constant throughout the experiment.

5. Conclusions

To summarize our conclusions: (i) There are two CP models, the classical I−S model and the I−I*−S model involving isolated spin clusters, each governed by a different set of parameters. (ii) It is difficult to predict in advance which model will be better for the quantification of a particular CP signal. (iii) The right CP model can be identified by careful inspection of the CP kinetic curve for very short contact times. (iv) CP intensities within the same spectrum and between different spectra can only be compared on the basis of CP amplitudes I_0, calculated by fitting the CP kinetic functions to variable-contact-time results. (v) The analysis of the CP kinetics provides relaxation, spin-diffusion, and cross-polarization parameters, which contain valuable information on molecular structure and dynamics in the solid state. (vi) For a better understanding of the CP kinetics, especially in complex materials, variable-contact-time experiments should be supported by depolarization, TORQUE, and relaxation measurements.

6. Acknowledgments

We are grateful to the British Council and the Polish State Committee for Scientific Research for support within the projects WAR/992/131 and 4P05B13115.

7. References

(1) Pines, A.; Gibby, M. G.; Waugh, J. S. *J. Chem. Phys.* **1973**, *59*, 569−590.
(2) Hartmann, S. R.; Hahn, E. L. *Phys. Rev.* **1962**, *128*, 2042−2053.
(3) Yannoni, C. S. *Acc. Chem. Res.* **1982**, *15*, 201−208.
(4) Fyfe, C. A. *Solid State NMR for Chemists*; C.F.C. Press: Ontario, Canada, 1983.
(5) Fukushima, E.; Roeder, S. B. W. *Experimental Pulse NMR. A Nuts and Bolts Approach*; Addison-Wesley: Reading, MA, 1981.
(6) Harris, R. K. *Nuclear Magnetic Resonance Spectroscopy. A Physicochemical View*; Pitman: London, 1983.
(7) Stejskal, E. O.; Memory, J. D. *High-Resolution NMR in the Solid State. Fundamentals of CP/MAS*; Oxford University Press: Oxford, 1994.
(8) Michel, D.; Engelke, F. In *Solid-State NMR III: Organic Matter*; Blümich, B., Ed.; Springer-Verlag: Berlin, 1994; Vol. 31.
(9) Abragam, A. *The Principles of Nuclear Magnetism*; Clarendon Press: Oxford, 1983.
(10) Goldman, M. *Spin Temperature and Nuclear Magnetic Resonance in Solids*; Oxford University Press: Oxford, 1970.
(11) Mehring, M. *High-Resolution NMR Spectroscopy in Solids*, 2nd ed.; Springer-Verlag: New York, 1983.
(12) Slichter, C. P. *Principles of Magnetic Resonance*, 3rd ed.; Springer-Verlag: New York, 1989.
(13) Gerstein, B. C.; Dybowski, C. R. *Transient Techniques in NMR of Solids*; Academic Press: Orlando, FL, 1985.
(14) Hennel, J. W.; Klinowski, J. *Fundamentals of Nuclear Magnetic Resonance*; Longman: Harlow, U.K., 1993.
(15) Kolodziejski, W.; Klinowski, J. *Chem. Phys. Lett.* **1995**, *247*, 507−509.
(16) Kolodziejski, W.; Corma, A.; Wozniak, K.; Klinowski, J. *J. Phys. Chem.* **1996**, *100*, 7345−7351.
(17) Blasco, T.; Pérez-Pariente, J.; Kolodziejski, W. *Solid State NMR* **1997**, *8*, 185−194.
(18) Walter, T. H.; Turner, G. L.; Oldfield, E. *J. Magn. Reson.* **1988**, *76*, 106−120.
(19) Kolodziejski, W.; Kasprzycka-Guttman, T. *Solid State NMR* **1998**, *11*, 177−180.
(20) Fülber, C.; Demco, D. E.; Blümich, B. *Solid State NMR* **1996**, *6*, 213−223.
(21) Van Vleck, J. H. *Phys. Rev.* **1948**, *74*, 1168−1183.
(22) Rocha, J.; Kolodziejski, W.; He, H. Y.; Klinowski, J. *J. Am. Chem. Soc.* **1992**, *114*, 4884−4888.
(23) Kolodziejski, W.; He, H. Y.; Klinowski, J. *Chem. Phys. Lett.* **1992**, *191*, 117−124.
(24) Kolodziejski, W.; Klinowski, J. *J. Magn. Reson.* **1992**, *99*, 611−614.

(25) Ernst, H.; Fenzke, D.; Pfeifer, H. *Ann. Phys. (Leipzig)* **1981**, *38*, 257−270.
(26) Schulze, D.; Ernst, H.; Fenzke, D.; Meiler, W.; Pfeifer, H. *J. Phys. Chem.* **1990**, *94*, 3499−3502.
(27) McBrierty, V. J.; Douglas, D. C. *Macromol. Rev. Part D, J. Polym. Sci.* **1981**, *16*, 295−366.
(28) Kaplan, J. I.; Garroway, A. N. *J. Magn. Reson.* **1982**, *49*, 464−475.
(29) Tekely, P.; Gérardy, V.; Palmas, P.; Canet, D.; Retournard, A. *Solid State NMR* **1995**, *4*, 361−367.
(30) Voelkel, R. *Angew. Chem., Int. Ed. Engl.* **1988**, *27*, 1468−1483.
(31) Müller, L.; Kumar, A.; Baumann, T.; Ernst, R. R. *Phys. Rev. Lett.* **1974**, *32*, 1402−1406.
(32) Hester, R. K.; Ackerman, J. L.; Cross, V. R.; Waugh, J. S. *Phys. Rev. Lett.* **1975**, *34*, 993−995.
(33) Suter, D.; Ernst, R. R. *Phys. Rev.* **1985**, *B32*, 5608−5627.
(34) Hagaman, E. W.; Ho, P. C.; Brown, L. L.; Schell, F. M.; Woody, M. C. *J. Am. Chem. Soc.* **1990**, *112*, 7445−7450.
(35) Naito, A.; McDowell, C. A. *J. Chem. Phys.* **1986**, *84*, 4181−4186.
(36) Takegoshi, K.; McDowell, C. A. *J. Chem. Phys.* **1987**, *86*, 6077−6084.
(37) Levitt, M. H.; Suter, D.; Ernst, R. R. *J. Chem. Phys.* **1986**, *84*, 4243−4255.
(38) Wu, X. L.; Zhang, S. M.; Wu, X. W. *Phys. Rev.* **1988**, *B37*, 9827−9829.
(39) Wu, X. L.; Zhang, S. M. *Chem. Phys. Lett.* **1989**, *156*, 79−81.
(40) Maricq, M. M.; Waugh, J. S. *J. Chem. Phys.* **1979**, *70*, 3300−3316.
(41) Alemany, L. B.; Grant, D. M.; Alger, T. D.; Pugmire, R. J. *J. Am. Chem. Soc.* **1983**, *105*, 6697−6704.
(42) Wu, X. L.; Zilm, K. W. *J. Magn. Reson.* **1991**, *93*, 265−278.
(43) Tian, F.; Cross, T. A. *J. Magn. Reson.* **1997**, *125*, 220−223.
(44) Pietraszkiewicz, M.; Pietraszkiewicz, O.; Kolodziejski, W.; Wozniak, K.; Feeder, N.; Benevelli, F.; Klinowski, J. *J. Phys. Chem.* **2000**, *B104*, 1921−1926.
(45) Kolodziejski, W.; Mazurek, A. P.; Kasprzycka-Guttman, T. *Chem. Phys. Lett.* **2000**, *328*, 263−269.
(46) Wu, X. L.; Zilm, K. W. *J. Magn. Reson.* **1993**, *A102*, 205−213.
(47) Wu, X. L.; Zilm, K. W. *J. Magn. Reson.* **1993**, *A104*, 119−122.
(48) Sangill, R.; Rastrup-Andersen, N.; Bildsøe, H.; Jakobsen, H. J.; Nielsen, N. C. *J. Magn. Reson.* **1994**, *A107*, 67−78.
(49) Wu, X. L.; Burns, S. T.; Zilm, K. W. *J. Magn. Reson.* **1994**, *A111*, 29−36.
(50) Kaflak, A.; Chmielewski, D.; Górecki, A.; Kolodziejski, W. *Solid State NMR* **1998**, *10*, 191−195.
(51) Kolodziejski, W.; Corma, A. *Solid State NMR* **1996**, *7*, 67−72.
(52) Hawkes, G. E.; Mantle, M. D.; Sales, K. D.; Aime, S.; Gobetto, R.; Groombridge, C. J. *J. Magn. Reson.* **1995**, *A116*, 251−254.
(53) Pratima, R.; Ramanathan, K. V. *J. Magn. Reson.* **1996**, *A118*, 7−10.
(54) Ando, S.; Harris, R. K.; Reinsberg, S. A. *J. Magn. Reson.* **1999**, *141*, 91−103.
(55) Kaflak-Hachulska, A.; Slosarczyk, A.; Kolodziejski, W. *Solid State NMR* **2000**, *15*, 237−238.
(56) Kaflak-Hachulska, A.; Kolodziejski, W. Manuscript in preparation.
(57) Stejskal, E. O.; Schaefer, J.; Waugh, J. S. *J. Magn. Reson.* **1977**, *28*, 105−112.
(58) Bertani, P.; Raya, J.; Reinheimer, P.; Gougeon, R.; Delmotte, L.; Hirschinger, J. *Solid State NMR* **1999**, *13*, 219−229.

CR000060N